


 Cite this: *RSC Adv.*, 2021, 11, 36689

Investigation on the upconversion luminescence and ratiometric thermal sensing of SrWO₄:Yb³⁺/RE³⁺ (RE = Ho/Er) phosphors

 Hang Liu, Xiukai Jian, Mingtai Liu, Kailin Wang, Guangyao Bai and Yuhong Zhang *

SrWO₄ phosphors doped with Ho³⁺(Er³⁺)/Yb³⁺ are successfully prepared by a high temperature solid-state reaction method. The upconversion (UC) luminescence properties of all the samples have been investigated under 980 nm excitation. Strong green emissions are obtained in the SrWO₄:Yb³⁺/Ho³⁺ and SrWO₄:Yb³⁺/Er³⁺ samples with the naked eyes. In a temperature range going from 303 K to 573 K, the UC emission spectra of the phosphors have been measured. Then the temperature sensing properties also have been discussed *via* fluorescence intensity ratio (FIR) technology. For the SrWO₄:Yb³⁺/Ho³⁺ phosphor, the FIR technologies based on thermal coupling levels (TCLs) (⁵F₄, ⁵F₅) and non-thermal coupling levels (non-TCLs) (⁵S₂, ⁵F₄/⁵F₅) are used for investigating the sensitivity. The results show that the maximum absolute sensitivity reaches 0.0158 K⁻¹ with non-TCLs. As for Yb³⁺/Er³⁺ codoped SrWO₄ phosphor, the maximum absolute sensitivity reaches 0.013 K⁻¹ with TCLs (²H_{11/2}, ⁴S_{5/2}) at a temperature of 513 K. These significant results demonstrate that the SrWO₄:Ho³⁺(Er³⁺)/Yb³⁺ phosphors are robust for optical temperature sensors.

Received 8th September 2021

Accepted 8th November 2021

DOI: 10.1039/d1ra06745a

rsc.li/rsc-advances

1. Introduction

As the basic parameter of thermodynamics, temperature measurement plays a vital role in scientific research, industrial production and medicine.¹ In recent years, much attention has been paid to non-contact temperature sensors based on rare earth (RE) ion activated luminescent materials.² Some UC luminescent materials with doping of RE³⁺ ions have been studied for temperature sensors.^{3–7} The FIR technology based on the measurement of the temperature-dependent FIR from two excited state energy levels of activators represents an accurate temperature measuring method, because the FIR from the thermally coupled levels (TCLs) of RE ions is independent of the excitation intensity fluctuations, external disturbance and spectrum losses. Thus, reasonable measurement accuracy and sensitivity could be obtained with this method. The variation of FIR is generally caused by a thermally induced population redistribution among the TCLs. And some RE ions have already been explored for designing FIR thermometry, such as Er³⁺, Tm³⁺, Ho³⁺ *et al.*^{8–13} The sensitivity is an important role of a temperature sensing device. The absolute sensitivity is defined as the rate of change of FIR with change in temperature relative to FIR. Basically, a larger energy gap between the TCLs benefits the enhancement of sensitivity. However, the largest energy mismatches between those TCLs cannot exceed 2000 cm⁻¹, so it is difficult for the further improvement of sensitivity. There is an urgent need to design a new temperature

measurement method to obtain high detecting sensitivity. Recently, a new kind of strategy has been proposed to solve the above drawback, which is based on FIR between the non-TCLs of the activators. The FIR derived from non-TCLs is also related to temperature. Compared with the FIR technique based on the TCLs, the FIR technique based on the non-TCLs is no longer limited by the energy gap. The Er³⁺ and Ho³⁺ ions also have non-TCLs pairs in addition to TCLs. So further investigation on temperature sensing properties of Er³⁺ and Ho³⁺ ions based on the FIR technology (TCLs and non-TCLs) is necessary.

Besides activators, temperature sensing properties of UC luminescent materials are also decided by host material. Among various hosts, tungstates have obtained much attention because of their brilliant physical and chemical stability, low phonon threshold energy, and high density.¹⁴ The Ln³⁺ ions also have high doped concentration in tungstates host. So the activators can emit intense and stable fluoresce even at high temperature.¹⁵ SrWO₄ belongs to a body-centered tetragonal system with scheelite crystal structure where WO₄²⁻ molecular ions are loosely bound to Sr²⁺ cations. It has been reported that SrWO₄ is an ideal host for optical temperature sensing materials. Recently, the temperature sensing properties of Ln³⁺ doped tungstates also have been studied. Pandey *et al.* report that the Er³⁺-Yb³⁺ co-doped SrWO₄ phosphor is a good optical temperature sensing material, and its maximum absolute sensitivity reaches 0.01498 K⁻¹.¹⁶ The high sensitivity of Tm³⁺/Yb³⁺ co-doped SrWO₄ phosphor for optical thermometry is synthesized by Song *et al.*, and when the temperature is 323 K, the absolute sensitivity reaches a maximum of 0.00617 K⁻¹.¹⁷ For Sm³⁺ doped SrWO₄ phosphor and Nd³⁺/Yb³⁺ co-doped

School of Electrical and Computer Engineering, Jilin Jianzhu University, Changchun 130118, China. E-mail: zhangyuhong@jlju.edu.cn; Liuhan76@163.com



SrWO₄ phosphor, they also have good temperature sensing performance.^{18,19} Note that, the SrWO₄ material is more suitable to be a UC fluorescence host for designing optical temperature sensor. However, as far as we know, the SrWO₄:Yb³⁺/Ho³⁺ phosphor for optical thermometry has not been investigated. There are even fewer reports on its optical thermometry using FIR technique based on the non-TCLs.

In this paper, the SrWO₄:Yb³⁺/RE³⁺ (RE = Er, Ho) phosphors are synthesized by a high temperature solid state reaction. The UC luminescence performances and temperature sensing properties are investigated under 980 nm excitation. The experimental results illustrate that the temperature sensitivity of our phosphors are better than the most reported Ho³⁺(Er³⁺) doped materials. The SrWO₄ doping Ho³⁺(Er³⁺) ions materials are optical temperature sensing material with good application value.

2. Experimental

2.1 Synthesis of the phosphor

The samples are designed according to the molar composition of Sr_{1-x-0.01}Yb_xHo_{0.01}WO₄ ($x = 0, 1\%, 2\%, 3\%, 4\%, 6\%, 10\%$) and Sr_{1-y-0.01}Yb_yEr_{0.01}WO₄ ($y = 0, 1\%, 2\%, 3\%, 4\%$), and synthesized by solid-state reaction method. High-purity SrCO₃ (99%), WO₃ (99.8%), Yb₂O₃ (99.99%), Ho₂O₃ (99.99%) and Er₂O₃ (99.99%) are purchased from Aladdin Chemical Reagent Co. Ltd (China). The raw materials are weighed by molar ratio and mixed together. The mixtures thoroughly are ground in a mortar of agate for 60 minutes. The ground mixture is transferred to a crucible ceramics and then heated it in a muffle furnace. First, the temperature rises to 900 °C by 10 °C min⁻¹. The samples are kept at 900 °C for 4 h. Next, temperature is increased by 5 °C min⁻¹ to 1100 °C and kept for 6 h. Finally the SrWO₄:Ho³⁺/Yb³⁺ and SrWO₄:Er³⁺/Yb³⁺ phosphors are obtained.

2.2 Measurement and characterization

The structural formation of the phosphors has been measured using an X-ray diffraction (Rigaku D/Max-2500) in the range of 15° to 80° (2θ), and its radiation source is Cu Kα ray of λ = 0.15406 nm. For morphology and size of the phosphors, the

field emission scanning electron microscope (FE-SEM, JEOL JEM-6700F) is used to perform. The UC emission spectra are recorded using the Zolix Omni-λ500 spectrometer under a 980 nm laser (MDL-III-980-2W, China) excitation. The samples are heated using an Orient KOJI TAP-02 high temperature thermometer, among a temperature range of 303 to 573 K, with a temperature control accuracy of 0.1 °C.

3. Result and discussion

3.1 Structural characterization

Fig. 1(a) shows the XRD patterns of the SrWO₄:Ho³⁺/Yb³⁺ phosphors. It can be seen that the diffraction peaks of the samples are very consistent with the standard card of SrWO₄ (JCPDS no. 08-0490). The sharp and strong diffraction peaks show that the synthesized samples are crystallized well. It also means that Sr²⁺ in the SrWO₄ lattice is substituted by Ho³⁺ and Yb³⁺ ions. The XRD patterns of the SrWO₄:Er³⁺/Yb³⁺ samples are shown in Fig. 1(b). The main diffraction peaks of samples are also consistent with the standard card of SrWO₄ (JCPDS no. 08-0490). But an extra weak peak at 29.3° appears in SrWO₄:1% Er³⁺, x%Yb³⁺ ($x = 2, 3, 4$) samples, which may be induced by the minor unreacted component of Yb₂O₃. Once the concentration of the Yb³⁺ ions is over 2%, a part of the Yb³⁺ ions will not be added in the lattice. In addition, the peak at 30° moves to a high angle direction with the concentration of Yb³⁺ ions increasing (see the illustration in Fig. 1(b)), which is attributed to the shrinkage of the crystal lattice caused by the doped Er³⁺ and Yb³⁺ ions substituting the Sr²⁺ sites. The ionic radius of Er³⁺, Yb³⁺ and Sr²⁺ (Er³⁺: 0.89 Å, Yb³⁺: 0.86 Å and Sr²⁺: 1.12 Å) are different, so the crystal lattice will produce deformation. The SEM images of SrWO₄:Ho³⁺(Er³⁺)/Yb³⁺ phosphor are shown in Fig. 2. It indicates that the size of the prepared phosphor is almost uniform.

3.2 Upconversion emission properties

Fig. 3(a) shows the UC emission spectrum of SrWO₄:1%Ho³⁺/2%Yb³⁺ phosphor from 500 to 800 nm under 980 nm excitation. Three characteristic emission bands are presented that the strong green emission (~540 nm) belongs to the radiative

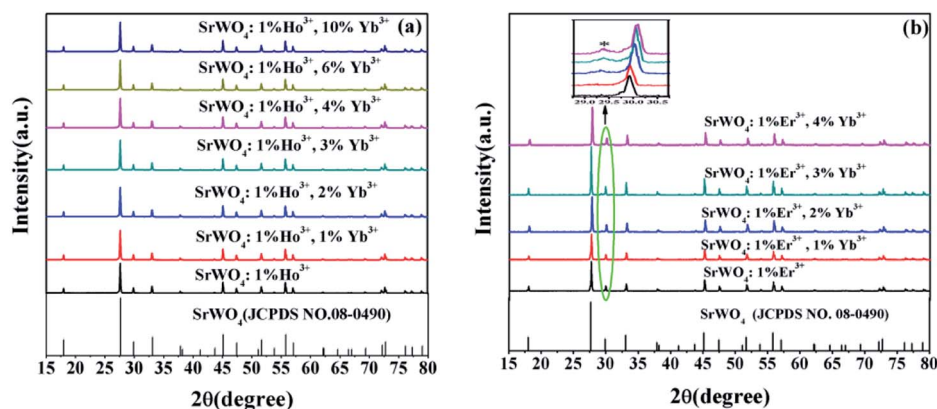


Fig. 1 XRD patterns of SrWO₄: (a) 1%Ho³⁺/x%Yb³⁺ ($x = 0, 1, 2, 3, 4, 6, 10$) phosphors. (b) 1%Er³⁺/x%Yb³⁺ ($x = 0, 1, 2, 3, 4$) phosphors.

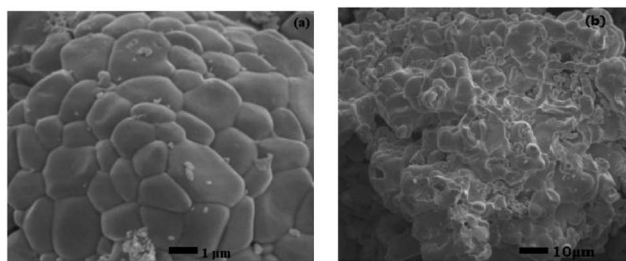


Fig. 2 SEM images of SrWO₄: (a) 1%Ho³⁺/2%Yb³⁺ phosphor. (b) 1%Er³⁺/1%Yb³⁺ phosphor.

transition from the ⁵S₂/⁵F₄ to ⁵I₈, the red emission (~663 nm) belongs to the radiative transition from ⁵F₅ to ⁵I₈ and the weak near infrared emission (~756 nm) corresponds to ⁵F₄ → ⁵I₇ energy level transition of Ho³⁺ ions. Fig. 3(b) shows the UC emission spectra of SrWO₄:1%Ho³⁺/x%Yb³⁺ (x = 0, 1, 2, 3, 4, 6, 10). It is seen that, the intensities of all the UC emission peaks reach maximum values at x = 2. But they decrease if the Yb³⁺ concentration is further increased up to 2%. The Yb³⁺ ion is a high-efficiency sensitizer for Ho³⁺ ion because it has larger absorption cross-sectional area at the near infrared. With increasing the Yb³⁺ ions concentration to 2%, the energy transfer process from Yb³⁺ to Ho³⁺ can be enhanced, resulting in higher UC emission intensity. However, with the further enhancement of the Yb³⁺ concentrations, the distance between the doping ions decreases with the increase of Yb³⁺ concentration. It induces more intense interaction among adjacent Yb³⁺ ions, which cause concentration quenching.²⁰

In order to explicate the possible UC emission process of the SrWO₄:Ho³⁺/Yb³⁺ sample, the dependence relation of the UC

emission intensity *via* pump power is measured. The relationship between UC emission intensity and pumping power can be described by the following eqn (1):²¹

$$I \propto P^n \quad (1)$$

where *I* is the UC emission intensity, *P* is the pumping power and *n* is the photon numbers which correspond to populate the upper emitting levels. Fig. 3(c) shows the log–log plot of intensity *versus* pump power and the slopes of the fitted lines of SrWO₄:1%Ho³⁺/2%Yb³⁺ sample. It can be seen that *n* values are 1.21, 1.24 and 2.27 for green (~540 nm), red (~663 nm), and near-infrared (~756 nm) emissions. It indicates that these UC emission processes are related to the two-photon processes. The energy level diagrams of Ho³⁺/Yb³⁺ ions and possible UC emission processes are shown in Fig. 3(d).

Under 980 nm excitation, the Yb³⁺ ion are excited from the ground state ²F_{7/2} to the excited state ²F_{5/2} by ground state absorption (GSA) process. Ho³⁺ ions are excited to the excited state levels mainly through the energy transfer (ET) process from Yb³⁺ to Ho³⁺. Through ET1 (²F_{5/2}(Yb³⁺) + ⁵I₈(Ho³⁺) → ²F_{7/2}(Yb³⁺) + ⁵I₆(Ho³⁺)), the Ho³⁺ ions are excited from the ⁵I₈ to the ⁵I₆ state.²² Some Ho³⁺ ions at ⁵I₆ state can nonradiatively (NR) relax to ⁵I₇ state, and then populating the ⁵F₅ state by excited state absorption (ESA) from ⁵I₇ to ⁵F₅. Ho³⁺ ions at ⁵I₆ state can continue to be excited into the ⁵S₂, ⁵F₄ coupling state by ET2 (²F_{5/2}(Yb³⁺) + ⁵I₆(Ho³⁺) → ²F_{7/2}(Yb³⁺) + ⁵S₂, ⁵F₄(Ho³⁺)). Subsequently, the Ho³⁺ ions at the ⁵S₂, ⁵F₄ coupling state will relax to the ⁵F₅ state by NR relaxation, and then a part of the Ho³⁺ ions at the ⁵F₅ state are transferred to the ⁵I₈ state, concurrently red light of 663 nm is emitted. The ⁵S₂, ⁵F₄ coupling state relax to the ⁵I₈ and ⁵I₇ states, resulting in high

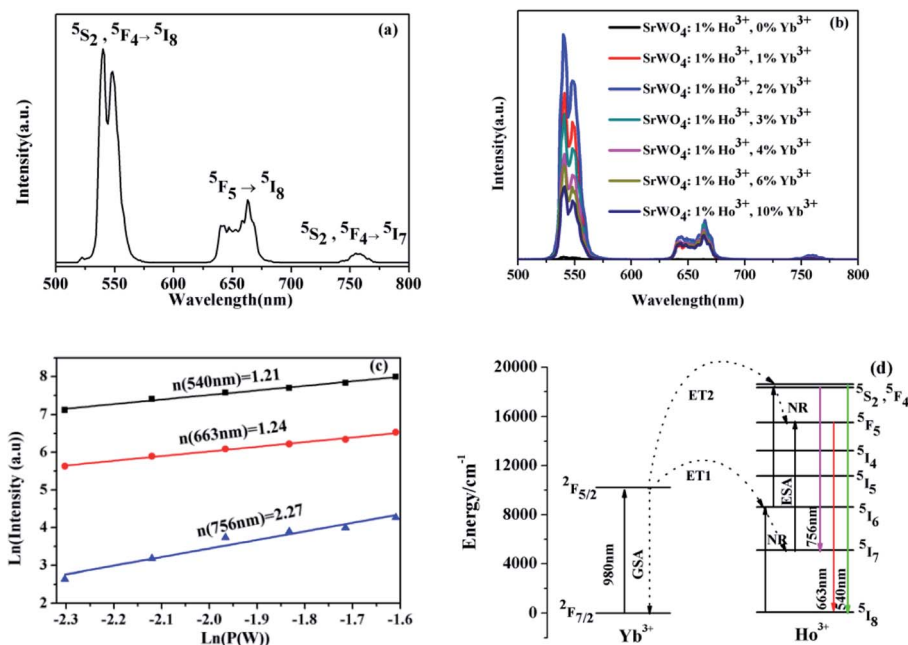


Fig. 3 (a). The emission spectrum of SrWO₄:1%Ho³⁺/2%Yb³⁺ phosphor from 500 to 800 nm under exciting at 980 nm. (b). The UC emission spectra of SrWO₄:1%Ho³⁺/x%Yb³⁺ (x = 0, 1, 2, 3, 4, 6, 10). (c). Log–log diagram of excitation power density and UC emission intensity. (d). The energy level diagrams of Ho³⁺/Yb³⁺ ions and possible UC emission processes.

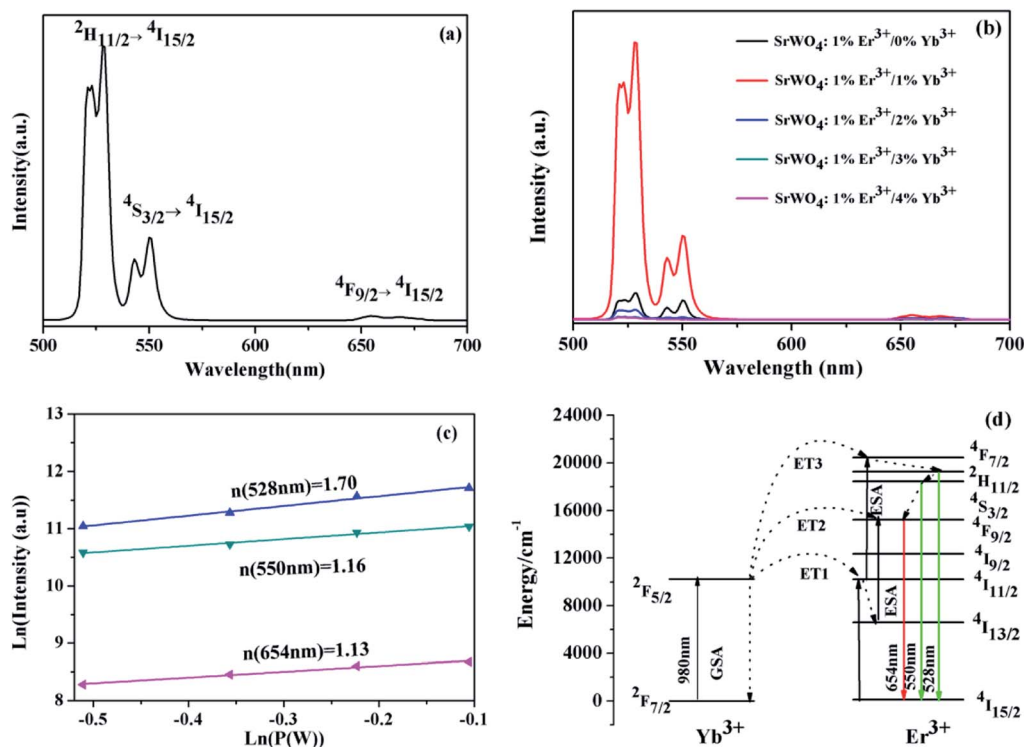


Fig. 4 (a). The UC emission spectrum of $\text{SrWO}_4:1\%\text{Er}^{3+}/1\%\text{Yb}^{3+}$ phosphor. (b). UC emission spectra of $\text{SrWO}_4:1\%\text{Er}^{3+}/x\%\text{Yb}^{3+}$ ($x = 0, 1, 2, 3, 4$). (c). Log-log relationship between pump power and UC emission intensity of $\text{SrWO}_4:1\%\text{Er}^{3+}/1\%\text{Yb}^{3+}$ phosphor. (d). The energy level diagrams of $\text{Er}^{3+}/\text{Yb}^{3+}$ ions and possible UC emission processes.

intensity green light (~ 540 nm) and low intensity red light (~ 756 nm), respectively.

The UC emission spectrum of $\text{SrWO}_4:1\%\text{Er}^{3+}/1\%\text{Yb}^{3+}$ phosphor is shown in Fig. 4(a). Two UC emission bands are exhibited, the strong green and the weak red emission, which can be attributed to the radiative transitions from ${}^2\text{H}_{11/2}/{}^4\text{S}_{3/2}$ to ${}^4\text{I}_{15/2}$ and the ${}^4\text{I}_{9/2} \rightarrow {}^4\text{I}_{15/2}$ of the Er^{3+} ions, respectively. Fig. 4(b) shows the UC emission spectra of $\text{SrWO}_4:1\%\text{Er}^{3+}/x\%\text{Yb}^{3+}$ ($x = 0, 1, 2, 3, 4$). It can be found that the intensities of two emission bands first increase and then decrease with increasing Yb^{3+} concentrations, and reach a maximum at $x = 1$. Once the concentration of Yb^{3+} is over 1%, the UC emission intensities rapidly decline. This is mainly attributed to that the energy transfer efficiency from Yb^{3+} to Er^{3+} ion decrease because the limit of the Yb^{3+} that can be stabilized into the matrix. As demonstrated by the extra peaks in the XRD patterns, when the concentration of the Yb^{3+} ions is over 2%, a part of the Yb^{3+} ions will not be added in the lattice.

The dependence relationship of the UC emission intensities of $\text{SrWO}_4:\text{Er}^{3+}/\text{Yb}^{3+}$ on pump power are shown in Fig. 4(c). For the emission ~ 528 nm, 550 nm and 654 nm, the slopes of the fitting experiment data are 1.70, 1.16 and 1.13, which is near 2. It indicates that all emission processes are related to the two-photon processes. Fig. 4(d) shows the energy level diagrams and possible UC emission processes of Er^{3+} and Yb^{3+} ion. Under 980 nm laser excitation, Yb^{3+} ions are excited from the ground state ${}^2\text{F}_{7/2}$ to the excited state ${}^2\text{F}_{5/2}$ by GSA process. The Er^{3+} ions are excited to the ${}^4\text{I}_{11/2}$ state from the ground state through the

ET1 (${}^2\text{F}_{5/2}(\text{Yb}^{3+}) + {}^4\text{I}_{15/2}(\text{Er}^{3+}) \rightarrow {}^2\text{F}_{7/2}(\text{Yb}^{3+}) + {}^4\text{I}_{11/2}(\text{Er}^{3+})$). After that, the Er^{3+} ions at ${}^4\text{F}_{7/2}$ state can be populated from the ${}^4\text{I}_{11/2}$ state by the ET3 (${}^2\text{F}_{5/2}(\text{Yb}^{3+}) + {}^4\text{I}_{11/2}(\text{Er}^{3+}) \rightarrow {}^2\text{F}_{7/2}(\text{Yb}^{3+}) + {}^4\text{F}_{7/2}(\text{Er}^{3+})$). The ${}^2\text{H}_{11/2}$ and ${}^4\text{S}_{3/2}$ states are populated from the ${}^4\text{F}_{7/2}$ state owing to the NR relaxation, and then the Er^{3+} ions at ${}^2\text{H}_{11/2}$ and ${}^4\text{S}_{3/2}$ states relax to the ${}^4\text{I}_{15/2}$ state, leading to the green UC emissions (528 nm and 550 nm). The Er^{3+} ions at ${}^4\text{I}_{11/2}$ state can relax to the ${}^4\text{I}_{13/2}$ state through the multiphonon relaxation (MPR) process, and then the Er^{3+} ions at ${}^4\text{I}_{13/2}$ state are excited to the ${}^4\text{F}_{9/2}$ by ET2 (${}^2\text{F}_{5/2}(\text{Yb}^{3+}) + {}^4\text{I}_{13/2}(\text{Er}^{3+}) \rightarrow {}^2\text{F}_{7/2}(\text{Yb}^{3+}) + {}^4\text{F}_{9/2}(\text{Er}^{3+})$). Meanwhile, the ${}^4\text{F}_{9/2}$ state can be also populated from the ${}^4\text{S}_{3/2}$ state through the NR relaxation. The Er^{3+} at the ${}^4\text{F}_{9/2}$ state will transit to the ${}^4\text{I}_{15/2}$ state and thus emitted the red light (~ 654 nm).

3.3 Optical temperature-sensing properties

For investigating the optical temperature sensing characteristics of $\text{SrWO}_4:\text{Ho}^{3+}/\text{Yb}^{3+}$ phosphor, the emission spectra of the $\text{SrWO}_4:\text{Ho}^{3+}/\text{Yb}^{3+}$ sample are measured at different temperature. As shown in Fig. 5(a), it can be seen that the UC emission intensities of all emission band decrease with the temperature increasing. The possible reason is thermal quenching effect.²³ But the decreasing rate of the different emission band is different. Fig. 5(b) shows the UC emission intensity variation of 540 nm (${}^5\text{S}_2, {}^5\text{F}_4 \rightarrow {}^5\text{I}_8$) and 756 nm (${}^5\text{S}_2, {}^5\text{F}_4 \rightarrow {}^5\text{I}_7$) with temperature increasing. It is clearly observed that the UC emission intensity at 756 nm drops much more slowly than that at 540 nm with the temperature increasing. By considering the

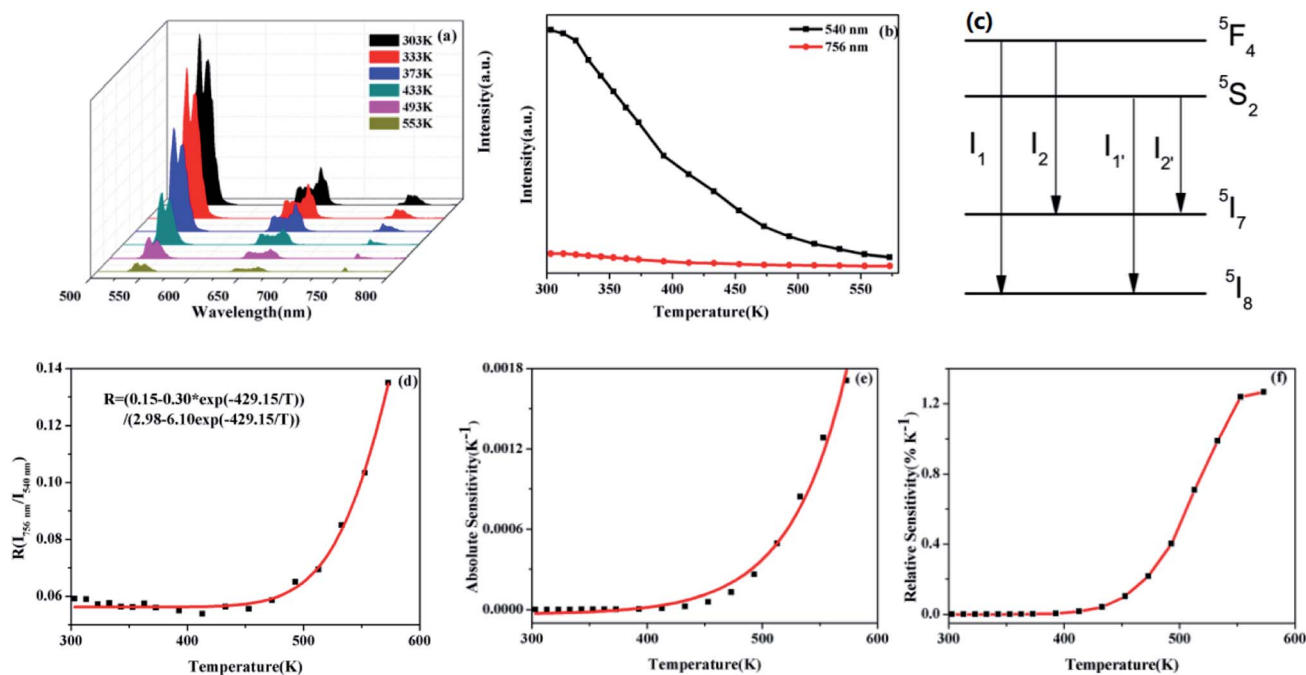


Fig. 5 (a). Temperature-dependent on UC emission spectra of $\text{SrWO}_4:1\%\text{Ho}^{3+}/2\%\text{Yb}^{3+}$ phosphor at 303–573 K. (b). The emission intensity of $\text{SrWO}_4:1\%\text{Ho}^{3+}/2\%\text{Yb}^{3+}$ phosphor center at 540 nm and 756 nm change in the range 303–573 K. (c) Four-level simplified diagram of transitions from adjacent excited levels to two lower levels. (d) The FIR ($I_{756 \text{ nm}}/I_{540 \text{ nm}}$). (e) the absolute sensitivity based on the $I_{756 \text{ nm}}/I_{540 \text{ nm}}$. (f) the relative sensitivity based on the $I_{756 \text{ nm}}/I_{540 \text{ nm}}$.

thermalization between $^5\text{S}_2$ and $^5\text{F}_4$ levels, the FIR of the UC emission from ($^5\text{F}_4, ^5\text{S}_2$) \rightarrow $^5\text{I}_8$ and ($^5\text{F}_4, ^5\text{S}_2$) \rightarrow $^5\text{I}_7$ transitions can be analyzed by using a four-level system, which was introduced by González-Pérez *et al.*²⁴ as shown in Fig. 5(c). The $^5\text{S}_2$, $^5\text{F}_4$, $^5\text{I}_7$ and $^5\text{I}_8$ levels form a four-level system. The emission intensity is proportional to the population of each energy level and the population of the excited state relates to the temperature. So the FIR can be expressed by the following eqn (2).²⁵

$$\text{FIR}_1 = \frac{I_{756 \text{ nm}}}{I_{540 \text{ nm}}} = \frac{C_1 + C_2 \exp(-\Delta E/kT)}{C_3 + C_4 \exp(-\Delta E/kT)} \quad (2)$$

where C_1 , C_2 , C_3 and C_4 are constants about spontaneous emission rate, energy level degeneracy and emission energy. ΔE is the energy gap of the $^5\text{S}_2$ and $^5\text{F}_4$, k is the Boltzmann constant, and T is the absolute temperature. It can be seen in Fig. 5(d), the FIR of the $I_{756 \text{ nm}}/I_{540 \text{ nm}}$ regularly changes with the temperature increasing. It shows a nonlinear variation of FIR value at the temperature range 303 to 573 K. The eqn (2) is used to well fit the data, the C_1 , C_2 , C_3 , C_4 and ΔE are 0.15, -0.3 , 2.98, -6.1 and 429.15 cm^{-1} , respectively.

In the experiment, absolute sensitivity (S_a) is a non-negligible evaluation index of temperature, which indicates the absolute change of FIR in unit temperature, as shown in eqn (3).

$$S_a = \left| \frac{\text{dFIR}}{\text{dT}} \right| \quad (3)$$

Relative sensitivity (S_r) is also an important parameter that can be described as:

$$S_r = \left| \frac{1}{\text{FIR}} \frac{\text{dFIR}}{\text{dT}} \right| \quad (4)$$

S_a and S_r of the sample are shown in Fig. 5(e) and (f), which are fitted by eqn (3) and (4). The S_a increases with the temperature enhancement, reaching a maximum of 0.0017 K^{-1} at 573 K. While the maximum value of S_r is $1.27\% \text{ K}^{-1}$ at 573 K.

Fig. 6(a) shows that the emission intensities of the green and red band vary with temperature increasing. It can be seen that the intensity of red emission decreases more slowly than that of green emission. The energy levels $^5\text{S}_2$, $^5\text{F}_4$ and $^5\text{F}_5$ energy levels are far apart, and the particle population at the two energy levels do not follow the Boltzmann-type distribution. The $^5\text{S}_2$, $^5\text{F}_4$ and $^5\text{F}_5$ belong to non-TCLs. So the traditional FIR analysis method based on TCLs is not appropriate for the non-TCLs system. In the previous report, the relation of the non-TCLs FIR and temperature can be fitted by eqn (5).²⁶

$$\text{FIR}_2 = \frac{I_{540 \text{ nm}}}{I_{663 \text{ nm}}} = a + bT + cT^2 \quad (5)$$

Fig. 6(b) shows that the original data for the $I_{540 \text{ nm}}/I_{663 \text{ nm}}$ as a function of the temperature fitting with the eqn (5). Consequently the FIR based on $^5\text{S}_2, ^5\text{F}_4/^5\text{F}_5$ (Ho^{3+}) shows the significant temperature dependence and well fits the eqn (5). The curve of S_a and S_r by calculation and fitting are shown in Fig. 6(c) and (d). The S_a goes down with the increasing of temperature. The maximum S_a is 0.0158 K^{-1} at 303 K. While the S_r reaches a maximum of $0.41\% \text{ K}^{-1}$ at 393 K. The above analysis of the sensitivity of $\text{SrWO}_4:\text{Ho}^{3+}/$

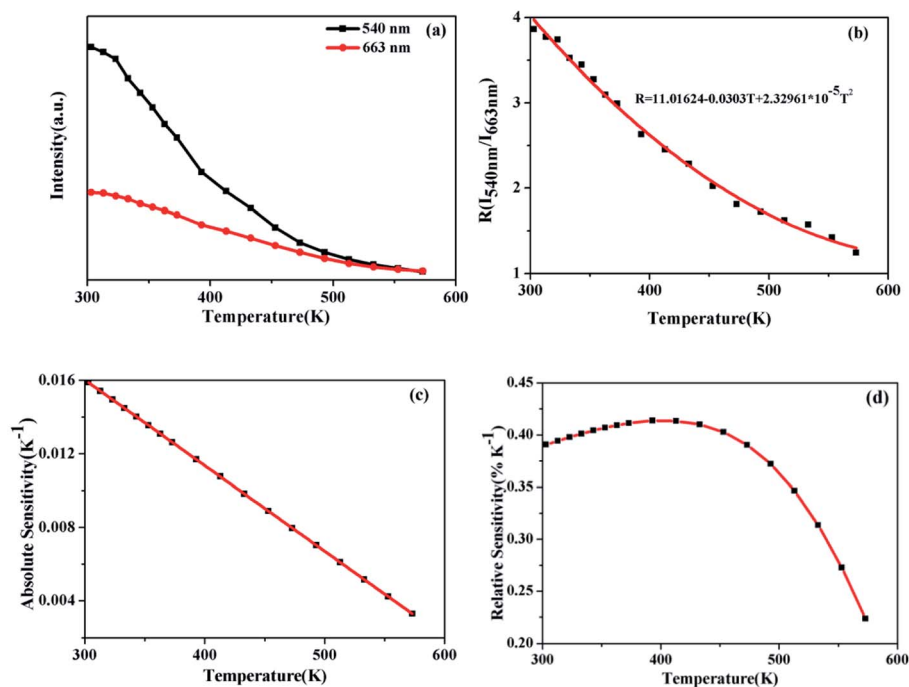


Fig. 6 (a) The emission intensity of $\text{SrWO}_4:1\%\text{Ho}^{3+}/2\%\text{Yb}^{3+}$ phosphor center at red (663 nm) and green (540 nm) changes with temperature. (b) The FIR ($I_{540\text{ nm}}/I_{663\text{ nm}}$), (c) the absolute sensitivity and (d) the relative sensitivity of $\text{SrWO}_4:\text{Ho}^{3+}/\text{Yb}^{3+}$ phosphor as a function of temperature.

Yb^{3+} based on the TCLs and the non-TCLs shows that the sample has high sensitivity and it has certain application value in optical temperature measurement.

Besides, the $\text{Er}^{3+}\text{-Yb}^{3+}$ co-doped SrWO_4 phosphor has also been studied for its sensing properties. As shown in Fig. 7(a),

the UC emission spectra of green light in the different temperature are recorded. The UC luminescence intensities of 528 nm and 550 nm (generated by $^2\text{H}_{11/2} \rightarrow ^4\text{I}_{15/2}$ and $^4\text{S}_{3/2} \rightarrow ^4\text{I}_{15/2}$) vary differently with the change of temperature. At 313 K, the intensity of the two emission bands is almost equal, with the

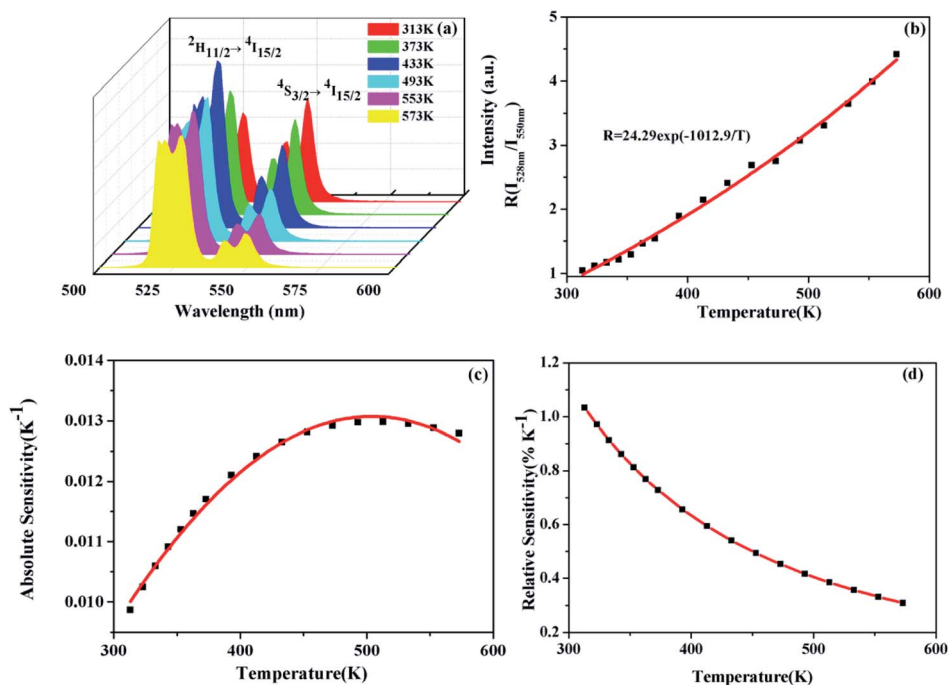


Fig. 7 (a) Temperature-dependent green UC emission spectra of $1\%\text{Er}^{3+}/1\%\text{Yb}^{3+}$ co-doped SrWO_4 phosphor at 313–573 K. (b) dependence of FIR for $I_{528\text{ nm}}/I_{550\text{ nm}}$ on absolute temperature. (c) and (d) The variation of absolute sensitivity and the relative sensitivity for $\text{SrWO}_4:1\%\text{Er}^{3+}/1\%\text{Yb}^{3+}$ phosphor with temperature between 313 K and 573 K.

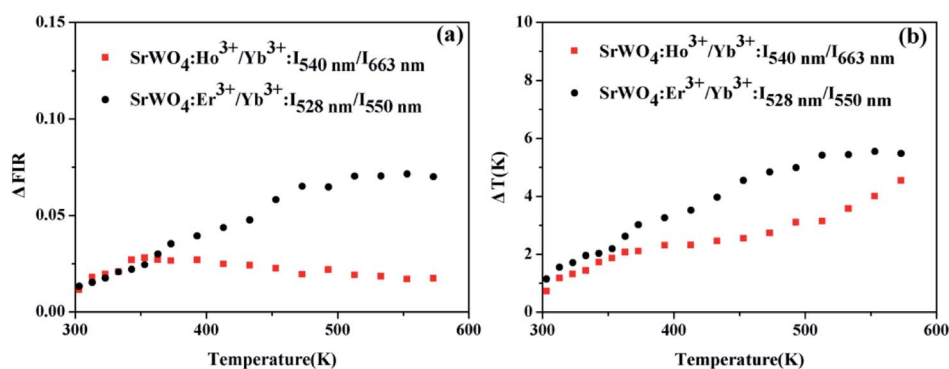


Fig. 8 (a) Δ FIR and (b) Δ T of $\text{SrWO}_4:\text{Ho}^{3+}/\text{Yb}^{3+}$ based on the non-TCLs ($^5\text{S}_2$, $^5\text{F}_4/^5\text{F}_5$) and $\text{SrWO}_4:\text{Er}^{3+}/\text{Yb}^{3+}$ based on the TCLs ($^2\text{H}_{11/2}/^4\text{S}_{3/2}$) pair at 303–573 K.

temperature increasing, the luminescence intensity of the 528 nm emission band is gradually increased within 313–433 K, and that of the 550 nm emission band gradually decreases. Then, in the range of 433–573 K, as the temperature increasing, the intensities of two bands also decrease because of the non-radiative relaxation enhancement. But the luminescence intensity of the 550 nm emission band decreases faster than that of 528 nm emission band. When the temperature increases, the electrons at $^4\text{S}_{3/2}$ state are excited. The transition from $^4\text{S}_{3/2}$ to $^2\text{H}_{11/2}$ occurs. It indicates that the $^2\text{H}_{11/2}$ and $^4\text{S}_{3/2}$ states of Er^{3+} can be regarded as TCLs, and the electrons population at $^2\text{H}_{11/2}$ and the $^4\text{S}_{3/2}$ states follows the Boltzmann distribution. The FIR of TCLs can be expressed by the eqn (6):²⁷

$$\text{FIR} = \frac{I_{528 \text{ nm}}}{I_{550 \text{ nm}}} = C \exp\left(-\frac{\Delta E}{kT}\right) \quad (6)$$

The changing of FIR of $I_{528 \text{ nm}}/I_{550 \text{ nm}}$ with temperature is displayed in Fig. 7(b), which is fitted by eqn (6). According to the fitting curve of the experimental data, the calculated C value is 24.29 and $\Delta E/k$ is 1012.9, so the ΔE between $^2\text{H}_{11/2}$ and $^4\text{S}_{3/2}$ is 703.7 cm^{-1} , which is very close to the experiment value of 758 cm^{-1} , the latter is obtained from the UC emission spectrum. Fig. 7(c) shows the S_a of $\text{SrWO}_4:1\% \text{Er}^{3+}/1\% \text{Yb}^{3+}$

phosphor. The S_a of the phosphor increases at first and then decreases, reaching a maximum of 0.013 K^{-1} at 513 K. In Fig. 7(d) the S_r also is calculated, and the S_r reaches a maximum of $1.03\% \text{ K}^{-1}$ at 313 K.

In addition, thermal resolution (ΔT) is also a key parameter, which can be defined as:

$$\Delta T = \frac{\Delta \text{FIR}}{\text{FIR}} \frac{1}{S_r} = \frac{\Delta \text{FIR}}{S_a} \quad (7)$$

where Δ FIR is the uncertainty of FIR, S_r is the relative sensitivity, and S_a is the absolute sensitivity. The Δ FIR can be calculated by the following equation.

$$\Delta \text{FIR} = \frac{\sum_{i=1}^{i=n} |\text{FIR}_i - \overline{\text{FIR}}|}{n} \quad (8)$$

where $\overline{\text{FIR}}$ and the corresponding uncertainty Δ FIR are the average and the standard deviation values from 20 measurements at each temperature, FIR_i is the i -th FIR measured at the same temperature and n is the number of measurements.

For $\text{SrWO}_4:\text{Ho}^{3+}/\text{Yb}^{3+}$ phosphor, the thermal resolution of temperature measurement based on the non-TCLs ($^5\text{S}_2$, $^5\text{F}_4/^5\text{F}_5$) FIR has been investigated. While the thermal resolution of temperature measurement based on the TCLs ($^2\text{H}_{11/2}/^4\text{S}_{3/2}$) also has been discussed for $\text{SrWO}_4:\text{Er}^{3+}/\text{Yb}^{3+}$ phosphor. The values

Table 1 Comparison of the maximum sensitivity of $\text{Ho}^{3+}(\text{Er}^{3+})/\text{Yb}^{3+}$ doped in different material

Materials	Energy level	S_r (K^{-1})	S_a (K^{-1})	Reference
$\text{Bi}_2\text{SiO}_5:\text{Yb}^{3+}, \text{Tm}^{3+}$	$^3\text{F}_{3/2}/^1\text{G}_4$	1.95% (300 K)	0.0168 (300 K)	7
$\text{NaGdF}_4:\text{Er}^{3+}/\text{Yb}^{3+}$	$^2\text{H}_{11/2}/^4\text{S}_{3/2}$	1.29% (303 K)	0.0382 (363 K)	28
$\text{LaF}_3:\text{Er}^{3+}/\text{Yb}^{3+}$	$^2\text{H}_{11/2}/^4\text{S}_{3/2}$	$844/\text{T}^{-2}$ (150 K)	0.0025 (400 K)	29
$\text{Y}_2\text{O}_3:\text{Ho}^{3+}/\text{Yb}^{3+}/\text{Zn}^{3+}$	$^5\text{F}_3/^3\text{K}_8$	$1067.76/\text{T}^{-2}$ (299 K)	0.003 (673 K)	30
$\text{NaLa}(\text{MnO}_4)_2:\text{Sm}^{3+}/\text{Tb}^{3+}$	$^4\text{G}_5/2/3/2\text{D}_4$	1.93 (498 K)	0.119 (265 K)	31
$\text{BaY}_2\text{Si}_3\text{O}_{10}:\text{Ho}^{3+}/\text{Yb}^{3+}$	$^5\text{F}_5/5\text{S}_2, ^5\text{F}_4$	0.49% (298 K)	0.023 (298–448 K)	32
$\text{BaY}_2\text{Si}_3\text{O}_{10}:\text{Er}^{3+}/\text{Yb}^{3+}$	$^4\text{F}_9/2/2\text{H}_{11/2}$	0.78% (298 K)	0.091 (298 K)	32
$\text{LaAlO}_3:\text{Er}^{3+}/\text{Yb}^{3+}$	$^2\text{H}_{11/2}/^4\text{S}_{3/2}$	$575.27/\text{T}^{-2}$ (281 K)	0.0032 (281 K)	33
$\text{NaY}(\text{WO}_4)_2:\text{Er}^{3+}/\text{Yb}^{3+}$	$^2\text{H}_{11/2}/^4\text{S}_{3/2}$	$1043.12/\text{T}^{-2}$ (133 K)	0.0112 (515 K)	34
$\text{SrWO}_4:\text{Er}^{3+}/\text{Yb}^{3+}$	$^2\text{H}_{11/2}/^4\text{S}_{3/2}$	1.03% (313 K)	0.013 (513 K)	This work
$\text{SrWO}_4:\text{Ho}^{3+}/\text{Yb}^{3+}$	$^5\text{S}_2/5\text{F}_4$	1.27% (573 K)	0.0017 (573 K)	This work
$\text{SrWO}_4:\text{Ho}^{3+}/\text{Yb}^{3+}$	$^5\text{S}_2, ^5\text{F}_4/5\text{F}_5$	0.41% (393 K)	0.0158 (303 K)	This work

of Δ FIR and ΔT are presented among the range of 303–573 K in Fig. 8(a) and (b), respectively. It can be seen that the Δ FIR of $\text{SrWO}_4:\text{Ho}^{3+}/\text{Yb}^{3+}$ is lower than that of $\text{SrWO}_4:\text{Er}^{3+}/\text{Yb}^{3+}$. At 303 K, the ΔT of $\text{SrWO}_4:\text{Ho}^{3+}/\text{Yb}^{3+}$ and $\text{SrWO}_4:\text{Er}^{3+}/\text{Yb}^{3+}$ have the minimum values of 0.72 K and 1.14 K, respectively. The values of ΔT become increasingly with the temperature enhancement. Therefore, the samples have better accuracy at lower temperature.

In order to correctly evaluate experimental results, the other materials doped with different RE ions are compared in Table 1. It can clearly conclude that the sensitivity of our sample is higher than that of the most of samples in the table.

4. Conclusion

In conclusion, the $\text{SrWO}_4:\text{Ho}^{3+}(\text{Er}^{3+})/\text{Yb}^{3+}$ phosphors are successfully prepared by solid state reaction method. The UC luminescence properties of $\text{SrWO}_4:\text{Ho}^{3+}(\text{Er}^{3+})/\text{Yb}^{3+}$ samples are investigated under 980 nm excitation. Furthermore, the temperature sensing properties of the $\text{Ho}^{3+}:^5\text{S}_2/^5\text{F}_4$ (TCLs), $\text{Er}^{3+}:^2\text{H}_{11/2}/^4\text{S}_{3/2}$ (TCLs) and the $\text{Ho}^{3+}:^5\text{S}_2, ^5\text{F}_4/^5\text{F}_5$ (non-TCLs) are investigated in the temperature range of 303–573 K. Specifically, the absolute sensitivity value reaches 0.0158 K^{-1} at 303 K for $\text{Ho}^{3+}:^5\text{S}_2, ^5\text{F}_4/^5\text{F}_5$ (non-TCLs) and the relative sensitivity value reaches 0.41% at 393 K, which is superior to most optical temperature sensing materials doped with RE³⁺ ions. It means that the $\text{SrWO}_4:\text{Ho}^{3+}/\text{Yb}^{3+}$ can achieve higher absolute sensitivity by FIR of non-TCLs, as well as it has potential application in optical temperature sensors.

Conflicts of interest

There are no conflicts to declare.

Acknowledgements

This work was supported by Natural Science Foundation of China (Grant No: 61705077); Science Foundation of Jilin Province Education Department (JJKH20190853KJ); Project of Jilin Provincial Science and Technology Department (No: 20190303064SF, 20200403072SF); Project of Jilin Province Development and Reform Commission (2019C048-4, 2020C021-5).

References

- 1 X. F. Wang, Q. Liu, Y. Y. Bu, C. S. Liu, T. Liu and X. H. Yan, Optical temperature sensing of rare-earth ion doped phosphors, *RSC Adv.*, 2015, 5(105), 86219–86236.
- 2 M. Back, E. Casagrande, E. Trave, D. Cristofori, E. Ambrosi, F. Dallo, M. Roman, J. Ueda, J. Xu, S. Tananbe, A. Benedetti and P. Riello, Confined-Melting-Assisted Synthesis of Bismuth Silicate Glass-Ceramic Nanoparticles: Formation and Optical Thermometry Investigation, *ACS Appl. Mater. Inter.*, 2020, 12, 55195–55204.
- 3 S. Balabhadra, M. L. Debasu, C. D. S. Brites, R. A. S. Ferreira and L. D. Carlos, Upconverting Nanoparticles Working as Primary Thermometers in Different Media, *J. Phys. Chem. C.*, 2017, 121(25), 13962–13968.
- 4 M. Back, J. Ueda, M. G. Brik and S. Tananbe, Pushing the Limit of Boltzmann Distribution in Cr³⁺-Doped CaHfO₃ for Cryogenic Thermometry, *ACS Appl. Mater. Inter.*, 2020, 12(34), 38325–38332.
- 5 A. Ćirić, T. Gavrilović and M. D. Dramićanin, Luminescence Intensity Ratio Thermometry With Er³⁺: Performance Overview, *Crystals*, 2021, 11(2), 189.
- 6 M. Back, E. Casagrande, C. A. Brondin, E. Ambrosi, D. Cristofori, J. Ueda, S. Tanabe, E. Trave and P. Riello, Lanthanide-Doped Bi₂SiO₅@SiO₂ Core-Shell Upconverting Nanoparticles for Stable Ratiometric Optical Thermometry, *ACS Appl. Nano Mater.*, 2020, 3, 2594–2604.
- 7 E. Casagrande, M. Back, D. Cristofori, J. Ueda, S. Tanabe, S. Palazzolo, F. Rizzolio, V. Canzonieri, E. Trave and P. Riello, Upconversion-mediated Boltzmann thermometry in double-layered Bi₂SiO₅:Yb³⁺,Tm³⁺@SiO₂ hollow nanoparticles, *J. Mater. Chem. C*, 2020, 8, 7828–7836.
- 8 S. S. Zhou, S. Jiang, X. T. Wei, Y. H. Chen, C. K. Duan and M. Yin, Optical thermometry based on upconversion luminescence in Yb³⁺/Ho³⁺ co-doped NaLuF₄, *J. Alloys Compd.*, 2014, 588, 654–657.
- 9 M. Back, J. Ueda, J. Xu, D. Murata, M. G. Brik and S. Tanabe, Ratiometric Luminescent Thermometers with a Customized Phase-Transition-Driven Fingerprint in Perovskite Oxides, *ACS Appl. Mater. Inter.*, 2019, 11, 38937–38945.
- 10 S. A. Wade, S. F. Collins and G. W. Baxter, Fluorescence intensity ratio technique for optical fiber point temperature sensing, *J. Appl. Phys.*, 2003, 94(8), 4743–4756.
- 11 M. Back, J. Ueda, H. Nambu, M. Fujita, A. Yamamoto, H. Yoshida, H. Tanaka, M. G. Brik and S. Tanabe, Boltzmann Thermometry in Cr³⁺-Doped Ga₂O₃ Polymorphs: The Structure Matters, *Adv. Optical Mater.*, 2021, 9, 2100033.
- 12 Y. Zhao, X. Wang, Y. Zhang, Y. Li and X. Yao, Optical temperature sensing of up-conversion luminescent materials: Fundamentals and progress, *J. Alloy Cod.*, 2020, 817, 152691.
- 13 M. Back, J. Ueda, J. Xu, K. Asami, M. G. Brik and S. Tananbe, Effective Ratiometric Luminescent Thermal Sensor by Cr³⁺-Doped Mullite Bi₂Al₄O₉ with Robust and Reliable Performances, *Adv. Optical Mater.*, 2020, 8(11), 2000124.
- 14 C. Shivakumara, R. Saraf, S. Behera, N. Dhananjaya and H. Nagabhushana, Scheelite-type MWO₄ (M = Ca, Sr, and Ba) nanophosphors: Facile synthesis, structural characterization, photoluminescence, and photocatalytic properties, *Mater. Res Bull.*, 2015, 61, 422–432.
- 15 A. Y. Lan, B. Li, H. Shen and J. L. Zhang, SrWO₄:Ho³⁺, Yb³⁺, Tm³⁺ microspheres with white-light emission: synthesis and luminescence, *J. Mater. Sci.: Mater. Electron.*, 2015, 26(3), 1695–1699.
- 16 A. Pandey, V. K. Rai, V. Kumar, V. Kumar and H. C. Swart, Upconversion based temperature sensing ability of Er³⁺-Yb³⁺ codoped SrWO₄: An optical heating phosphor, *Sens. Actuators, B*, 2015, 209, 352–358.

- 17 H. L. Song, C. Wang, Q. Han, X. Y. Tang, W. C. Yan, Y. F. Chen, J. F. Jiang and T. G. Liu, Highly sensitive Tm³⁺/Yb³⁺codoped SrWO₄ for optical thermometry, *Sens. Actuators, A*, 2018, **271**, 278–282.
- 18 H. L. Song, Q. Han, C. Wang, X. Y. Tang, W. C. Yan, Y. F. Chen, X. R. Zhao, J. F. Jiang and T. G. Liu, Optical temperature sensing properties of Sm³⁺ doped SrWO₄ phosphor, *Opt. Mater.*, 2018, **78**, 402–406.
- 19 H. L. Song, Q. Han, X. Y. Tang, X. R. Zhao, K. Ren and T. G. Liu, Nd³⁺/Yb³⁺ codoped SrWO₄ for highly sensitive optical thermometry based on the near infrared emission, *Opt. Mater.*, 2018, **84**, 263–267.
- 20 F. Huang, Y. Gao, J. C. Zhou, J. Xu and Y. S. Wang, Yb³⁺/Er³⁺ co-doped CaMoO₄: a promising green upconversion phosphor for optical temperature sensing, *J. Alloys Compd.*, 2015, **639**, 325–329.
- 21 J. Zhou, Y. Q. Chen, R. S. Lei, H. P. Wang, Q. G. Zhu, X. M. Wang, Y. Q. Wu, Q. H. Yang and S. Q. Xu, Excellent photoluminescence and temperature sensing properties in Ho³⁺/Yb³⁺ codoped (Y_{0.88}La_{0.09}Zr_{0.03})₂O₃ transparent ceramics, *Ceram. Int.*, 2019, **45**(6), 7696–7702.
- 22 X. N. Chai, J. Li and X. S. Wang, Upconversion Luminescence and Temperature Sensing Properties of Ho³⁺/Yb³⁺-Codoped ZnWO₄ Phosphors Based on Fluorescence Intensity Ratios, *RSC Adv.*, 2017, **64**, 40046–40052.
- 23 L. Lei, D. Q. Chen, C. Li, F. Huang, J. J. Zhang and S. Q. Xu, Inverse thermal quenching effect in lanthanide-doped upconversion nanocrystals for anti-counterfeiting, *J. Mater. Chem. C*, 2018, **6**(20), 5427–5433.
- 24 P. Haro-González, S. F. León-Luis, S. González-Pérez and I. R. Martín, Analysis of Er³⁺ and Ho³⁺ codoped fluoroindate glasses as wide range temperature sensor, *Mater. Res. Bull.*, 2011, **46**, 1051–1054.
- 25 P. Du, L. H. Luo and J. S. Yu, Low-temperature thermometry based on upconversion emission of Ho/Yb-codoped Ba_{0.77}Ca_{0.23}TiO₃ ceramics, *J. Alloys Compd.*, 2015, **632**, 73–77.
- 26 H. Y. Lu, H. Y. Hao, G. Shi, Y. C. Gao, R. X. Wang, Y. L. Song, Y. X. Wang and X. R. Zhang, Optical temperature sensing in β-NaLuF₄:Yb³⁺/Er³⁺/Tm³⁺ based on thermal, quasi-thermal and non-thermal coupling levels, *RSC Adv.*, 2016, **6**, 55307–55311.
- 27 X. N. Chai, J. Li, X. S. Wang, Y. X. Li and X. Yao, Color-tunable upconversion photoluminescence and highly performed optical temperature sensing in Er³⁺/Yb³⁺ codoped ZnWO₄, *Opt. Express*, 2016, **24**(20), 22438–22447.
- 28 J. M. Wang, H. Lin, Y. Cheng, X. S. Cui, Y. Gao, Z. L. Ji, J. Xu and Y. S. Wang, A novel high-sensitive upconversion thermometry strategy: Utilizing synergistic effect of dual-wavelength lasers excitation to manipulate electron thermal distribution, *Sens. Actuators, B*, 2019, **278**, 165–171.
- 29 H. J. Zhang, X. B. Dong, L. Y. Jiang, Y. Yang, X. R. Cheng and H. M. Zhao, Comparative analysis of upconversion emission of LaF₃:Er/Yb and LaOF:Er/Yb for temperature sensing, *J. Mol. Struct.*, 2020, **1206**, 127665.
- 30 A. Pandey and V. K. Ray, Improved Luminescence and Temperature Sensing Performance of Ho³⁺, Yb³⁺, Zn²⁺:Y₂O₃ Phosphor, *Dalton Trans.*, 2013, **42**, 11005–11011.
- 31 Y. Zhu, Q. Meng, W. Sun and S. Lü, Sm³⁺, Tb³⁺ co-doped NaLa(MoO₄)₂ temperature sensing materials based on the fluorescence intensity ratio, *J. Alloys Compd.*, 2019, **784**, 456–462.
- 32 H. Q. Ge and J. Zhang, Investigation on luminescence properties of BaY₂Si₃O₁₀:Er³⁺/Ho³⁺-Yb³⁺ for optical temperature sensing, *J. Mater. Sci.: Mater. Electron.*, 2018, **29**, 20033–20039.
- 33 G. F. Liu, L. L. Fu, Z. Y. Gao, X. X. Yang, Z. L. Fu, Z. Y. Wang and Y. M. Yang, Investigation on the Temperature Sensing Behavior in Yb³⁺ Sensitized Er³⁺ doped Y₂O₃, YAG and LaAlO₃ Phosphors, *RSC Adv.*, 2015, **5**(64), 51820–51827.
- 34 P. Du, L. H. Luo and J. S. Yu, Upconversion emission, cathodoluminescence and temperature sensing behaviors of Yb³⁺ ions sensitized NaY(WO₄)₂:Er³⁺ phosphors, *Ceram. Int.*, 2015, **42**(5), 5635–5641.